Received: 27 February 2024 | Revised: 31 May 2024 | Accepted: 14 June 2024 | Published online: 21 June 2024

RESEARCH ARTICLE

Medinformatics
2024, Vol. 1(3) 152–163
DOI: 10.47852/bonviewMEDIN42022711

BON VIEW PUBLISHING

ADME, Molecular Targets, Docking, and Dynamic Simulation Studies of Phytoconstituents of *Cymbopogon citratus* (DC.)

Iseoluwa Isaac Ajayi[1], Toluwase Hezekiah Fatoki[2,*], Ayodele Sunday Alonge[1], Ibrahim Olabayode Saliu[3], Olalekan Elijah Odesanmi[4], Jude Akinyelu[2] and Oluwaferanmi Excel Oke[1]

[1]*Department of Biological Sciences, Bamidele Olumilua University of Education, Science and Technology, Nigeria*

[2]*Department of Biochemistry, Federal University Oye-Ekiti, Nigeria*

[3]*Department of Genetics, Washington University School of Medicine, USA*

[4]*Department of Biochemistry, Ekiti State University, Nigeria*

Abstract: *Cymbopogon citratus* (DC) Stapf. is utilized in both culinary and medicinal contexts, wherein its extracts demonstrate a range of therapeutic properties, including antidiabetic, antioxidant, and anti-inflammatory activities. This investigation aimed to computationally analyze phytochemicals of *C. citratus*, evaluating their pharmacokinetics and binding dynamics. The findings revealed a combination of high and low gastrointestinal absorption (GIA) for *C. citratus* (DC.) phytochemicals, with some exhibiting permeability across the blood-brain barrier (BBB). Xanthine dehydrogenase/oxidase (XDH) emerged as the primary human molecular target of *C. citratus* phytocompounds, while XDH and matrix metalloproteinase-9 (MMP9) have central connectivity in the protein interaction network. Orientin has best binding affinity with XDH (−9.083 kcal.mol^{-1}) and MMP9 (−9.051 kcal.mol^{-1}). Molecular dynamic simulations indicated the favorable stability and interactions of XDH with orientin and quercetin, respectively. In summary, this investigation underscores the potential of twenty-six (26) phytochemicals in *C. citratus* extract to combat cancer and neurodegenerative diseases through mechanisms targeting XDH and MMP9.

Keywords: *C. citratus*, phytoconstituents, orientin, XDH, MMP9, cancer, neurodegenerative diseases

1. Introduction

Cymbopogon citratus (DC) Stapf., generally referred to as lemongrass, is a member of graminoid plant family, that is extensively dispersed in humid and subhumid regions of the world including Nigeria. It found application as food and ethnomedicinal ingredient [1, 2]. The extracts of *C. citratus* possess wide array of healing properties which include antioxidant, antidiabetic, antimicrobial, anti-inflammatory, anti-flu, anti-tussive, anti-fever, and anti-malarial, activities [1–4], as well as exhibiting insecticidal and insect-repellent effects against various insects such as mosquitoes, fruit flies (*Drosophila melanogaster*), sand flies, and houseflies [5]. The biological or therapeutic effects of *C. citratus* extracts have been attributed to the rich phytochemical compounds it contained such as specifically phenolics, flavonoids, and terpenoids [6].

In studies focusing on antidiabetic properties, *C. citratus* extracts have demonstrated inhibition of some carbohydrate enzymes such as alpha-glucosidase and alpha-amylase [1, 2, 7], with molecular docking studies reporting binding affinities of approximately −6.00 kcal/mol [2]. Additionally, research has shown *that* streptozotocin-induced type 1 diabetes could be mitigated by the *C. citratus* extracts by improving the activity of the antioxidant enzymes, liver biomarkers, levels of malondialdehyde, and glutathione thereby increasing anti-inflammatory responses, as well as reducing pro-inflammatory cytokine levels [8]. In anti-malarial studies, molecular docking simulations of *C. citratus* phytochemicals indicated −7.8 kcal/mol as the binding affinity of swertiajaponin for *Plasmodium falciparum* merozoite surface protein 1, while quercetin demonstrates significant binding affinities of 8.3 and 6.8 kcal/mol with *P. falciparum* circumsporozoite protein and *P. falciparum* erythrocyte membrane protein 1 respectively [4].

This study adopts a holistic approach to comprehend the intrinsic therapeutic significance of *C. citratus*, which may not be feasible through wet lab experiments alone, by employing computational methods. These insights could potentially expand

*Corresponding author: Toluwase Hezekiah Fatoki, Department of Biochemistry, Federal University Oye-Ekiti, Nigeria. Email: toluwase.fatoki@fuoye.edu.ng

the medicinal applications of this plant. Computational approaches have been increasingly utilized to investigate phytochemicals from medicinal plants, aiming to unravel their pharmacokinetics and molecular targets involved in ameliorating specific human diseases [9, 10]. The rationale for conducting this present study lies in the potential therapeutic benefits of *C. citratus* phytochemicals including antimicrobial, antioxidant, anti-inflammatory, and anticancer activities. Understanding the ADME properties of phytochemicals from *C. citratus* is crucial for predicting their bioavailability, distribution in the body, metabolism, and elimination, which are pivotal factors in determining their efficacy and safety as potential therapeutic agents. Additionally, identifying the molecular targets of these phytochemicals provides insights into their mechanisms of action, enabling the rational design of novel drugs or therapeutic interventions. Overall, investigating the ADME properties, molecular targets, docking, and molecular dynamics (MD) of phytochemicals from *C. citratus* holds significant promise for the development of novel drugs with enhanced efficacy and reduced side effects for the treatment of various diseases. Thus, the objective of this study was to computationally examine *C. citratus* phytochemicals, evaluating their pharmacokinetics, molecular binding affinity, and dynamics in simulated physiological condition.

2. Materials and Methods

2.1. Phytochemicals structure

The chemicals present in *C. citratus* were obtained from the previously published works [4, 8]. The name of each phytochemical was searched on the PubChem database on NCBI, and each chemical structure was obtained in SMILES and SDF formats.

2.2. Pharmacokinetics prediction

The *in silico* pharmacokinetics properties of the phytochemicals compounds were conducted on the SwissADME webserver at default settings [11] by using the SMILES of each of phytochemicals. SwissADME provides information about chemical compound physicochemical and pharmacokinetics properties.

2.3. Molecular target prediction

Target prediction analysis was conducted on the SEA Search webserver [12], using the SMILES of each of phytochemicals. The result indicating human targets were selected and used for further analyses.

2.4. Gene-gene association prediction

The gene IDs of the predicted human targets of phytochemicals present in *Cymbopogon citratus* were collated and used to query the STRING database [13], and gene-gene (or protein-protein) network of interactions was obtained.

2.5. Gene enrichment analysis

The gene IDs of predicted human targets were used to query the eXpression2Kinases (X2K) Webserver [14], and the regulatory network consisting of kinases, transcription factors, and protein-protein interaction was obtained. X2K provide information on the signaling pathway that linked to the overall predicted targets activity.

2.6. Molecular docking analyzes

Molecular docking was executed based on the reported protocol [15]. Two target proteins (Xanthine dehydrogenase/oxidase (XDH) with UniProt ID: P47989, and matrix metalloproteinase-9 (MMP9) with UniProt ID: P14780) were used for the molecular docking. The target proteins AlphaFold 3D structures were obtained from the UniProt database. The SMILES of the phytochemicals (ligands) of *Cymbopogon citratus* were converted to 3D structure and optimized on the ACDLab/ChemSketch v2021 and file format conversion was done using PyMol software. The proteins and ligands were prepared for docking in pdbqt format using AutoDock Tools v1.5.6 [16]. The molecular docking was implemented from the command prompt using AutoDock Vina v1.2.3 [17, 18]. Following docking, ezLigPlot on the ezCADD webserver [19] was used to visualize the ligand-protein interaction.

2.7. Molecular dynamics simulation

Two ligand-protein complexes with the best binding affinity were used for this analysis. Maestro's protein preparation wizard was used preprocessing. Desmond software by Schrödinger LLC v2021-1 was used to implement the system simulation of 100 ns [15, 20, 21]. The system setup includes OPLS-2005 force field, orthorhombic box with TIP3P water model containing 0.15 M NaCl counter ions to established physiological conditions, with a 1 atm pressure and 300 K temperature for the simulation. The models underwent energy minimization before simulation. During full system simulation, the trajectories were saved at every 100 ps. The post-simulation trajectories analysis was conducted to determine (i) root-mean-square deviation (RMSD) which measures the average distance between the atoms of a reference structure and those of a trajectory ensemble, (ii) root-mean-square fluctuation (RMSF) which quantifies the flexibility or mobility of individual atoms or residues within a biomolecular system throughout the simulation, and (iii) protein-ligand contact profile which shows interactions such as hydrogen bonds, hydrophobic and electrostatic interactions. Additionally, prime molecular mechanics/generalized Born surface area (MM-GBSA) was used to determine the binding free energy (ΔG^{bind}) [15, 21, 22]. MM-GBSA calculates the binding free energy of a protein-ligand complex, which represents the overall stability of the complex in solution, as follows:

$$\begin{aligned} \text{MM} - \text{GBSA}\Delta G^{bind} = {} & \Delta G^{Coulomb} + \Delta G^{Covalent} \\ & + \Delta G^{Hbond} + \Delta G^{Lipo} + \Delta G^{Packing} \\ & + \Delta G^{SolvGB} + \Delta G^{vdW} \end{aligned}$$

3. Results

The investigation of phytochemical compounds in *Cymbopogon citratus* (DC.) presented in Figure 1 revealed diverse pharmacokinetic characteristics, as shown in Table 1. Some phytoconstituents, including cymbopogonol, orientin, chlorogenic acid, lycopene, swertiajaponin, rutin, and rosmarinic acid, exhibited low gastrointestinal absorption (GIA), while others demonstrated high GIA. Cymbopogonol exhibited poor solubility, lycopene was insoluble, and the rest were soluble. Additionally, linalool, ferulic acid, geraniol, citronellal, hydroquinone, catechol, and p-coumaric acid were predicted to permeate the blood-brain

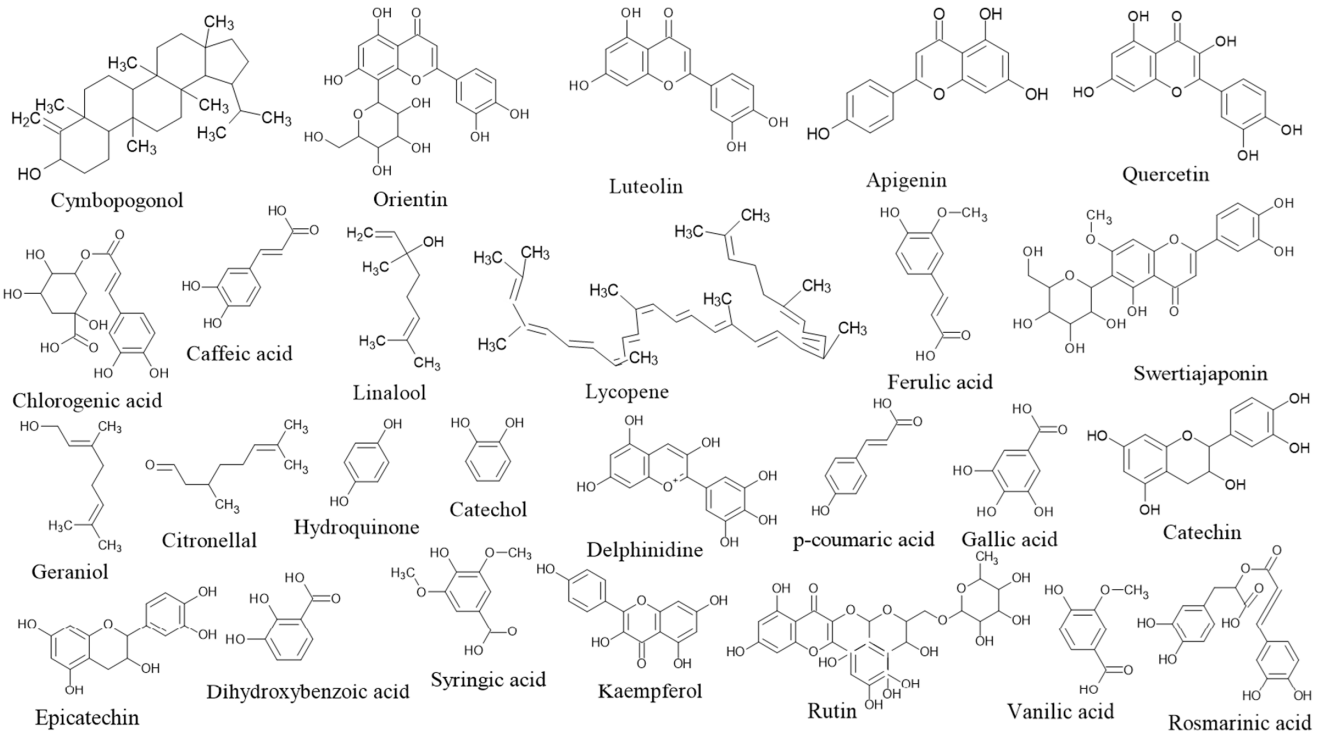

Figure 1. Structures of the 26 phytochemicals of *Cymbopogon citratus* (DC.)

barrier (BBB), with most compounds capable of inhibiting CYP3A4 and few acting as substrates of P-glycoprotein (P-gp).

The predicted targets in Table 2 showed that the most common human molecular targets of *C. citratus* phytocompounds include XDH/oxidase, NADPH oxidase 4, squalene monooxygenase (SQLE), aldo-keto reductase family 1 member B10, and atromal cell-derived factor 1. These results were ranked based on maximum Tanimoto coefficient and p-value, which are indicators of similarity between query compounds with the database references. Cytochrome P450 1B1 and broad substrate specificity ATP-binding cassette transporter were identified as key proteins connecting metabolism to functional activity pathways, interacting with XDH, MMP9, SQLE, and estrogen receptor beta, as depicted in Figure 2(A). The results of target protein network of *C. citratus* phytocompounds revealed biosignaling pathways that involve kinases such as MAPK1, MAPK3, MAPK8, MAPK14, CDK1, CDK4, GSK3B, AKT1, SYK, FYN, and transcription factors including RELA, HDAC2, EGR1, SUZ12, FOXA2, MYOD1, SREBF1, ONECUT1, and others, as shown in Figure 2(B and C).

The results of docking of *C. citratus* phytochemicals with XDH and MMP9, presented in Table 3, indicated orientin exhibited the highest binding affinity for XDH (−9.083 kcal.mol^{-1}), afterward quercetin (−8.748 kcal.mol^{-1}) and catechin (−8.476 kcal.mol^{-1}). Similarly, orientin showed the highest binding affinity for MMP9 (−9.051 kcal.mol^{-1}), afterward quercetin (−8.043 kcal.mol^{-1}). Overall, *C. citratus* phytochemicals showed good binding affinity for XDH compared to MMP9. The binding pose of complexes with high binding affinity that show the amino acid residues is depicted in Figure 3.

The results of the ligand-protein complexes MD simulations showed stability of the binding interaction of XDH with orientin and quercetin respectively as presented in Figure 4. For the orientin-XDH complex, the RMSD of the protein was 2.7 Å and the ligand was 3.5 Å over the 0–100 ns simulation period (Figure 4A). RMSF analysis showed maximal fluctuation at amino acid residues 190–200 (Figure 4B). Ligand-protein interactions involved amino acid residues such as GLU267, ASN351, ASP360, ASP429, and SER1226, contributing to hydrophobic interactions, hydrogen bonds, ionic interactions, and water bridges (Figure 4C). Similarly, for the quercetin-XDH complex, the RMSD of the protein was 2.40 Å and the ligand was 3.6 Å over the 0–100 ns simulation period (Figure 4D). RMSF analysis indicated maximal fluctuation at amino acid residues 190–200 (Figure 4E). Ligand-protein interactions involved amino acid residues such as LEU257, VAL259, GLU263, SER347, ILE353, and LEY404, contributing to various interactions (Figure 4F). Detailed ligand-protein atom interactions are presented in Figure 5.

The MD simulation results demonstrated suitable stability and interactions of orientin-XDH and quercetin-XDH complexes, with major amino acid residues contributing to their interactions. The MM-GBSA binding free energies for the complexes were computed at 0 ns (before simulation) and 100 ns (after simulation), as shown in Table 4. The results indicate that the binding energy ΔG^{bind} (Total) at 100 ns was lesser than at 0 ns for both the orientin-XDH complex (−54.338 to −46.531 kcal.mol^{-1}) and quercetin-XDH complex (−61.189 to −39.661 kcal.mol Protein), suggesting less stable energetics of the XDH-orientin and XDH-quercetin bindings over the 100 ns MDS duration.

4. Discussion

Cymbopogon citratus is a significant member of the Gramineae family, renowned for its diverse pharmacological properties. In this study, the phytoconstituents of *C. citratus* were computationally evaluated for their pharmacokinetic properties, molecular targets, gene signaling pathway kinases, transcription factors, binding affinity, and stability with XDH and MMP9.

Table 1. Predicted ADME properties of *Cymbopogon citratus* phytochemicals

SN	Ligands	PubChem ID	MW	MR	TPSA (Å^2)	Log P	ESOL Log S	ESOL Class	GIA	BBB permeant	P-gp	CYPs Inhibitor*	Lip	BS
			426.72	135.14	20.23	7.2	−8.3	Poorly soluble	Low	No	No	–	1	0.55
2	Orientin	5281675	448.38	108.63	201.28	−0.41	−2.7	Soluble	Low	No	No	–	2	0.17
3	Luteolin	5280445	286.24	76.01	111.13	1.73	−3.71	Soluble	High	No	No	a,d,e	0	0.55
4	Apigenin	5280443	270.24	73.99	90.9	2.11	−3.94	Soluble	High	No	No	a,d,e	0	0.55
5	Quercetin	5280343	302.24	78.03	131.36	1.23	−3.16	Soluble	High	No	No	a,d,e	0	0.55
6	Chlorogenic acid	1794427	354.31	83.5	164.75	−0.38	−1.62	Very soluble	Low	No	No	–	1	0.11
7	Caffeic acid	689043	180.16	47.16	77.76	0.93	−1.89	Very soluble	High	No	No	–	0	0.56
8	Linalool	6549	154.25	50.44	20.23	2.66	−2.4	Soluble	High	Yes	No	–	0	0.55
9	Lycopene	446925	536.87	188.23	0	11.9	−11.92	Insoluble	Low	No	Yes	–	2	0.17
10	Ferulic acid	445858	194.18	51.63	66.76	1.36	−2.11	Soluble	High	Yes	No	–	0	0.85
11	Swertiajaponin	442659	462.4	113.1	190.28	−0.02	−2.92	Soluble	Low	No	No	–	2	0.17
12	Geraniol	637566	154.25	50.4	20.23	2.78	−2.78	Soluble	High	Yes	No	–	0	0.55
13	Citronellal	7794	154.25	49.91	17.07	2.94	−2.88	Soluble	High	Yes	No	–	0	0.55
14	Hydroquinone	785	110.11	30.49	40.46	0.87	−1.45	Very soluble	High	Yes	No	e	0	0.55
15	Catechol	289	110.11	30.49	40.46	0.97	−1.63	Very soluble	High	Yes	No	e	0	0.55
16	Delphinidine	68245	338.7	84.05	134.52	−0.98	−3.16	Soluble	High	No	Yes	–	1	0.55
17	p-coumaric acid	637542	164.16	45.13	57.53	1.26	−2.02	Soluble	High	Yes	No	–	0	0.85
18	Gallic acid	370	170.12	39.47	97.99	0.21	−1.64	Very soluble	High	No	No	e	0	0.56
19	Catechin	9064	290.27	74.33	110.38	0.85	−2.22	Soluble	High	No	Yes	–	0	0.55
20	Epicatechin	72276	290.27	74.33	110.38	0.85	−2.22	Soluble	High	No	Yes	–	0	0.55
21	Dihydroxybenzoic acid	19	154.12	37.45	77.76	0.75	−1.89	Very soluble	High	No	No	e	0	0.56
22	Syringic acid	10742	198.17	48.41	75.99	0.99	−1.84	Very soluble	High	No	No	–	0	0.56
23	Kaempferol	5280863	286.24	76.01	111.13	1.58	−3.31	Soluble	High	No	No	a,d,e	0	0.55
24	Rutin	5280805	610.52	141.38	269.43	−1.29	−3.3	Soluble	Low	No	Yes	–	3	0.17
25	Rosmarinic acid	5281792	360.31	91.4	144.52	1.52	−3.44	Soluble	Low	No	No	–	0	0.56
26	Vanilic acid	8468	168.15	41.92	66.76	1.08	−2.02	Soluble	High	No	No	–	0	0.85

Note: Pharmacokinetics: Gastrointestinal absorption (GIA), P-glycoprotein (P-gp) substrate, Blood-brain barrier (BBB), *Inhibition of Cytochrome P450 (CYPs) type (a) CYP1A2, (b) CYP2C19, (c) CYP2C9, (d) CYP2D6, and (e) CYP3A4. **Physicochemical properties**: **Lipophilicity**: Consensus Log P. Molecular weight (MW), Total polar surface area (TPSA), Molar refractivity (MR). **Water Solubility:** ESOL Class, ESOL Log S. **Druglikeness**: Lipinski (Lip), Bioavailability Score (BS).

Table 2. Predicted molecular target

SN	Compound	Target description	Target gene code	p-value	MTC
1	Cymbopogonol	–	–	–	–
2	Orientin	Cyclic AMP-responsive element-binding protein 1	CREB1	2.927e-59	0.30
		ELAV-like protein 3	ELAVL3	2.548e-25	0.32
		Sodium/glucose cotransporter 2	SLC5A2	2.213e-150	0.43
		Xanthine dehydrogenase/oxidase	**XDH**	2.779e-29	0.45
3	Luteolin	Aldo-keto reductase family 1 member B10	**AKR1B10**	2.776e-15	1.00
		Arachidonate 5-lipoxygenase	ALOX5	7.883e-15	1.00
		Broad substrate specificity ATP-binding cassette transporter ABCG2	ABCG2	3.331e-16	1.00
		Cytochrome P450 1B1	CYP1B1	1.744e-46	1.00
		NADPH oxidase 4	**NOX4**	2.696e-24	1.00
		Xanthine dehydrogenase/oxidase	**XDH**	9.528e-52	1.00
4	Apigenin	Aldo-keto reductase family 1 member B10	**AKR1B10**	6.661e-16	1.00
		Cytochrome P450 1B1	CYP1B1	3.521e-56	1.00
		Estrogen receptor beta	ESR2	2.226e-32	1.00
		NADPH oxidase 4	**NOX4**	1.135e-21	1.00
		Xanthine dehydrogenase/oxidase	**XDH**	3.26e-43	1.00
5	Quercetin	Arachidonate 5-lipoxygenase	ALOX5	1.443e-18	1.00
		Cytochrome P450 1B1	CYP1B1	1.358e-45	1.00
		ELAV-like protein 3	ELAVL3	3.073e-96	1.00
		NADPH oxidase 4	**NOX4**	1.561e-25	1.00
		Xanthine dehydrogenase/oxidase	**XDH**	5.18e-44	1.00
6	Chlorogenic acid	Aldo-keto reductase family 1 member B10	AKR1B10	1.281e-23	0.91
		Amyloid-beta precursor protein	APP	3.291e-19	0.83
		Nuclear receptor subfamily 0 group B member 2	NR0B2	1.276e-48	0.34
		Stromal cell-derived factor 1	CXCL12	2.292e-49	0.36
7	Caffeic acid	Aldo-keto reductase family 1 member B10	AKR1B10	4.619e-28	0.56
		Carbonic anhydrase 6	CA6	4.062e-26	1.00
		Matrix metalloproteinase-9	MMP9	1.319e-21	1.00
		Nuclear receptor subfamily 0 group B member 2	NR0B2	9.731e-82	0.45
		Stromal cell-derived factor 1	CXCL12	4.45e-112	0.57
8	Linalool	Geranylgeranyl pyrophosphate synthase	GGPS1	7.666e-20	0.32
		Squalene monooxygenase	SQLE	5.719e-31	0.32
9	Lycopene	Geranylgeranyl pyrophosphate synthase	GGPS1	2.112e-30	0.41
		Squalene monooxygenase	SQLE	3.371e-39	0.41
10	Ferulic acid	Amyloid-beta precursor protein	APP	4.089e-79	0.79
		Carbonic anhydrase 6	CA6	2.276e-30	1.00
		Nuclear receptor subfamily 0 group B member 2	NR0B2	1.312e-75	0.42
		Stromal cell-derived factor 1	CXCL12	1.04e-177	0.69
		Tubulin beta-1 chain	TUBB1	1.102e-112	0.49
11	Swertiajaponin	Cyclic AMP-responsive element-binding protein 1	CREB1	1.079e-79	0.42
		Protein disulfide-isomerase	P4HB	2.868e-34	0.46
		Receptor-type tyrosine-protein phosphatase S	PTPRS	5.007e-40	0.43
		Sodium/glucose cotransporter 2	SLC5A2	1.089e-136	0.41
		Xanthine dehydrogenase/oxidase	XDH	1.297e-22	0.44
12	Geraniol	Geranylgeranyl pyrophosphate synthase	GGPS1	4.881e-70	0.48
		Lanosterol synthase	LSS	4.595e-18	0.38
		Squalene monooxygenase	SQLE	3.18e-67	0.62
13	Citronellal	Macrophage scavenger receptor types I and II	MSR1	6.315e-44	0.35
		Geranylgeranyl pyrophosphate synthase	GGPS1	1.595e-12	0.35
14	Hydroquinone	Carbonic anhydrase 3	CA3	1.786e-23	0.62
		Dihydropteridine reductase	QDPR	1.209e-17	0.35
		Estrogen receptor beta	ESR2	7.795e-35	0.57
		Myoglobin	MB	7.967e-22	0.42
		Succinate-semialdehyde dehydrogenase, mitochondrial	ALDH5A1	3.077e-50	0.40
15	Catechol	Carbonic anhydrase 5B, mitochondrial	CA5B	2.407e-08	1.00
		Dopamine beta-hydroxylase	DBH	8.027e-34	0.50
		Histone acetyltransferase KAT8	KAT8	6.482e-25	0.40
16	Delphinidine	ELAV-like protein 3	ELAVL3	2.897e-13	0.33
		Receptor-type tyrosine-protein phosphatase S	PTPRS	3.025e-06	0.30
17	p-coumaric Acid	Aldo-keto reductase family 1 member B1	AKR1B1	5.551e-16	1.00

(*Continued*)

Table 2. (*Continued*)

SN	Compound	Target description	Target gene code	p-value	MTC
		Carbonic anhydrase 5B, mitochondrial	CA5B	5.523e-27	1.00
		Estrogen receptor beta	ESR2	3.537e-13	1.00
		Nuclear receptor subfamily 0 group B member 2	NR0B2	3.76e-67	0.35
		Stromal cell-derived factor 1	CXCL12	1.069e-58	0.53
		Succinate-semialdehyde dehydrogenase, mitochondrial	ALDH5A1	3.987e-46	0.37
18	Gallic acid	Alpha-(1,3)-fucosyltransferase 7	FUT7	9.099e-79	1.00
		Carbonic anhydrase 3	CA3	1.854e-18	1.00
		Dipeptidyl peptidase 4	DPP4	0.8551	1.00
		Prolyl 4-hydroxylase subunit alpha-1	P4HA1	1.474e-56	0.32
		Thiopurine S-methyltransferase	TPMT	1.215e-87	0.47
19	Catechin	6-phosphogluconate dehydrogenase, decarboxylating	PGD	6.991e-56	0.60
		Alpha-(1,3)-fucosyltransferase 4	FUT4	6.014e-59	0.47
		Carbonic anhydrase 3	CA3	2.411e-11	1.00
		Placenta growth factor	PGF	4.035e-80	0.56
		Vascular endothelial growth factor A	VEGFA	5.484e-26	0.56
20	Epicatechin	6-phosphogluconate dehydrogenase, decarboxylating	PGD	6.991e-56	0.60
		Alpha-(1,3)-fucosyltransferase 4	FUT4	6.014e-59	0.47
		Carbonic anhydrase 3	CA3	2.411e-11	1.00
		Placenta growth factor	PGF	4.035e-80	0.56
21	Dihydroxybenzoic acid	Aldo-keto reductase family 1 member C2	AKR1C2	1.407e-81	0.40
		High mobility group protein B1	HMGB1	1.081e-42	0.53
		Alpha-ketoglutarate-dependent dioxygenase FTO	FTO	2.333e-37	0.53
22	Syringic acid	Carbonic anhydrase 7	CA7	7.772e-16	1.00
		Serine/threonine-protein kinase/endoribonuclease IRE1	ERN1	2.423e-77	0.50
		Stromal cell-derived factor 1	CXCL12	1.546e-58	0.41
		Thiopurine S-methyltransferase	TPMT	1.699e-87	0.48
		Tubulin beta-1 chain	TUBB1	1.913e-56	0.34
23	Kaempferol	Cyclic AMP-responsive element-binding protein 1	CREB1	5.513e-45	0.30
		Cystathionine beta-synthase	CBS	9.017e-51	0.45
		ELAV-like protein 3	ELAVL3	1.407e-81	0.78
		Protein disulfide-isomerase	P4HB	6.101e-41	0.52
		Receptor-type tyrosine-protein phosphatase S	PTPRS	5.492e-59	0.75
24	Rutin	Acetylcholinesterase	ACHE	0.1968	1.00
		Alpha-2C adrenergic receptor	ADRA2C	0.001543	1.00
		ELAV-like protein 3	ELAVL3	9.441e-51	0.49
		NADPH oxidase 4	NOX4	1.99e-18	0.75
		Neuromedin-U receptor 2	NMUR2	3.937e-30	1.00
		Protein disulfide-isomerase	P4HB	6.54e-73	1.00
		Xanthine dehydrogenase/oxidase	XDH	3.384e-26	0.66
25	Rosmarinic acid	Aldo-keto reductase family 1 member B1	AKR1B1	1.234e-12	1.00
		Aldo-keto reductase family 1 member B10	AKR1B10	3.454e-27	0.54
		Amyloid-beta precursor protein	APP	2.677e-34	0.59
		Estradiol 17-beta-dehydrogenase 2	HSD17B2	6.898e-06	1.00
		Interstitial collagenase	MMP1	2.882e-12	1.00
		Stromal cell-derived factor 1	CXCL12	8.102e-86	0.40
		Transthyretin	TTR	2.5e-18	1.00
26	Vanillic acid	7-dehydrocholesterol reductase	DHCR7	2.195e-44	0.41
		Hydroxycarboxylic acid receptor 3	HCAR3	1.121e-108	0.37
		Retinoic acid receptor beta	RARB	7.731e-74	0.46
		Stromal cell-derived factor 1	CXCL12	1.292e-127	0.61
		Thiopurine S-methyltransferase	TPMT	1.059e-78	0.44

The pharmacokinetics results revealed that most phytoconstituents of *C. citratus* exhibit moderate water solubility and GIA, with some capable of permeating the BBB. Orientin displayed low GIA possibly due to its large molecular size, with no predicted inhibitory effects on cytochromes (CYPs). However, quercetin showed high GIA, attributed to its molecular size and possible inhibitory effects on certain CYPs. GIA is crucial in drug efficacy as it dictates a drug's bioavailability, impacting the amount of administered dose reaching the bloodstream. Enhancement or inhibition of CYP activities can alter the drug metabolism profile, affecting either an increase in bioavailability or a decrease in efficacy [23]. Lower Log P values correspond to decreased toxicity of drug systems, with systems around a Log P value of 2.2 deemed more suitable for bioavailability in oral route of administration [24]. P-gp, a membrane transporter, plays a role in drug absorption and distribution by actively pumping

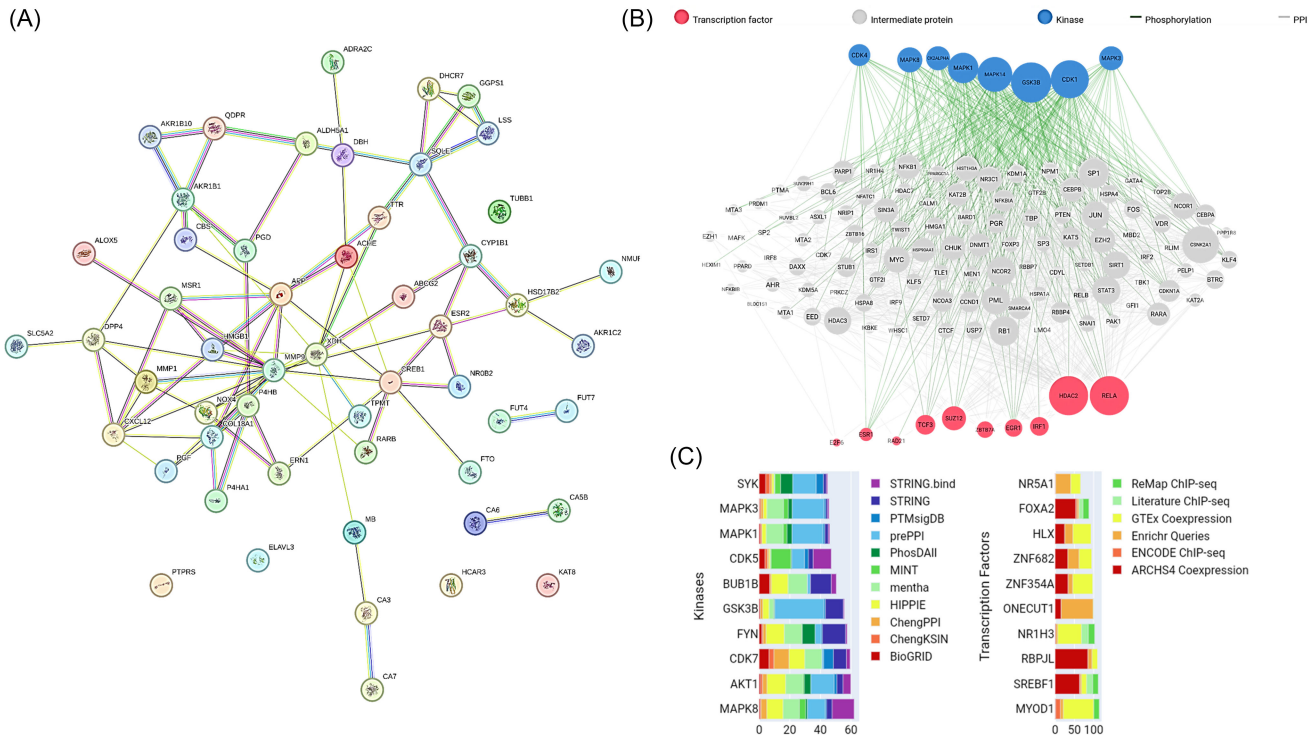

Figure 2. (A) Interaction network of *C. citratus* molecular targets. (B) Biosignaling network of predicted target genes. (C) Frequency of transcription factors and kinases associated with predicted target genes in biological library.

Table 3. Results of molecular docking

S.N	Phytochemicals	Binding affinity ΔG (kcal.mol^{-1})	
		XDH (AlphaFold ID: AF-P47989)	MMP9 (AlphaFold ID: AF-P14780)
1	Apigenin	**−8.337**	−7.144
2	Caffeic acid	−6.592	−5.981
3	Catechin	**−8.476**	−6.959
4	Catechol	−5.624	−5.231
5	Chlorogenic acid	−7.311	−6.638
6	Citronellal	−6.606	−5.259
7	Cymbopogonol	**−8.455**	−7.736
8	Delphinidine	**−8.247**	−7.799
9	Dihydroxybenzoic acid	−5.800	**−7.22**
10	Epicatechin	−7.464	−6.976
11	Ferulic acid	−6.298	−5.172
12	Gallic acid	−6.077	−5.895
13	Geraniol	−6.705	−5.629
14	Hydroquinone	−5.873	**−5.907**
15	Kaempferol	**−8.353**	−7.714
16	Linalool	−5.49	−4.786
17	Luteolin	**−8.208**	−7.656
18	Lycopene	−7.371	5.298
19	Orientin	**−9.083**	**−9.051**
20	p-coumaric acid	−6.722	−5.205
21	Quercetin	**−8.748**	**−8.043**
22	Rosmarinic acid	−8.033	−6.545
23	Rutin	−8.232	−7.185
24	Swertiajaponin	−7.725	−7.746
25	Syringic acid	−6.279	−5.042
26	Vanilic acid	−5.721	−5.217

Note: Docking parameter: XDH (P47989) [spacing: 0.875, npts: 106 × 90 × 100, center: −2.553 × 4.094 × −0.833] and MMP9 (P14780) [spacing: 0.875, npts: 96 × 80 × 126, center: −5.117 × −3.979 × −1.427].

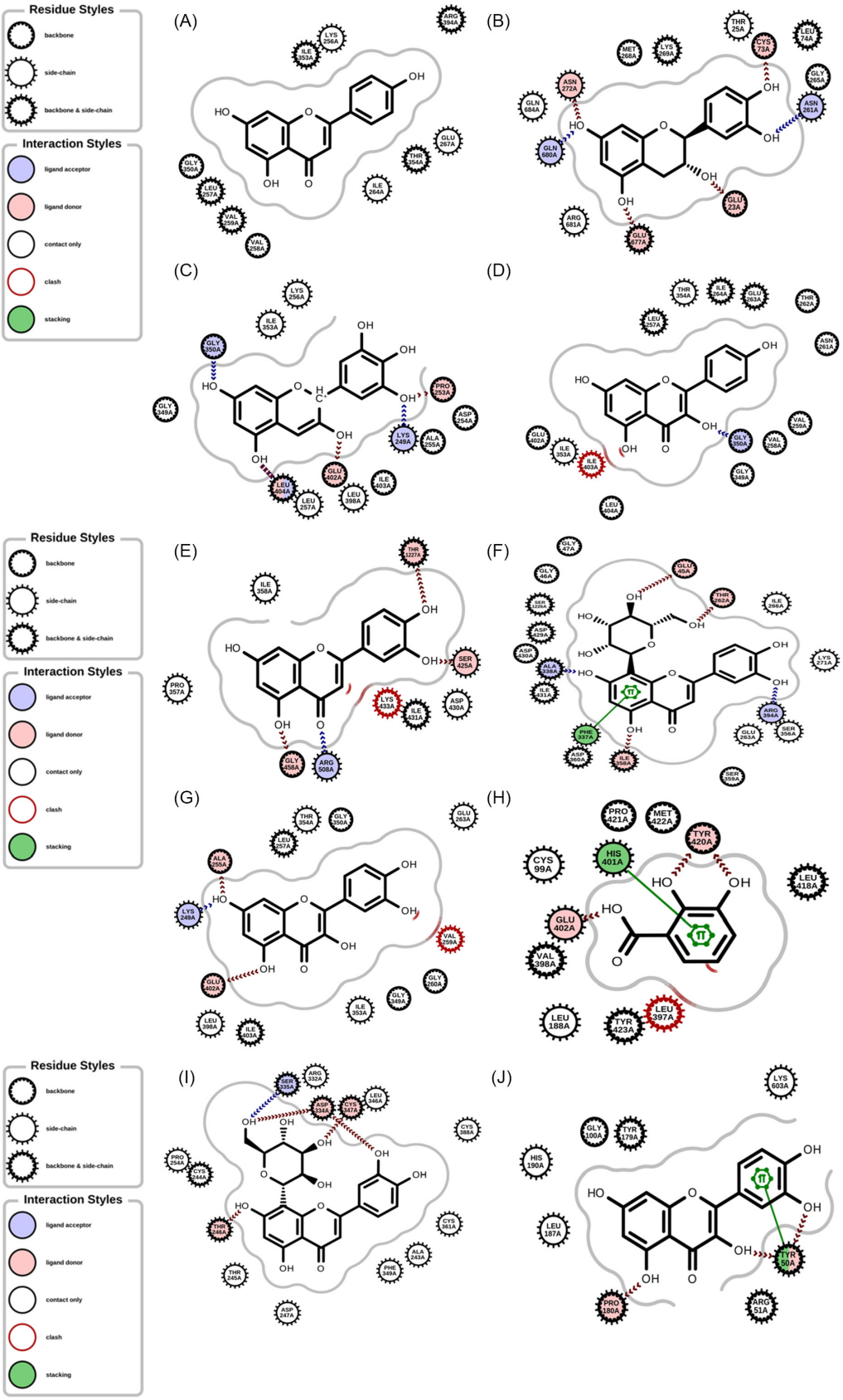

Figure 3. Interaction of the binding poses of (A) apigenin and P47989 (XDH). (B) Catechin and P47989 (XDH). (C) Delphinidine and P47989 (XDH). (D) Kaempferol and P47989 (XDH). (E) Luteolin and P47989 (XDH). (F) Orientin and P47989 (XDH). (G) Quercetin and P47989 (XDH). (H) Dihydroxybenzoic acid and P14780 (MMP9). (I) Orientin and P14780 (MMP9). (J) Quercetin and P14780 (MMP9).

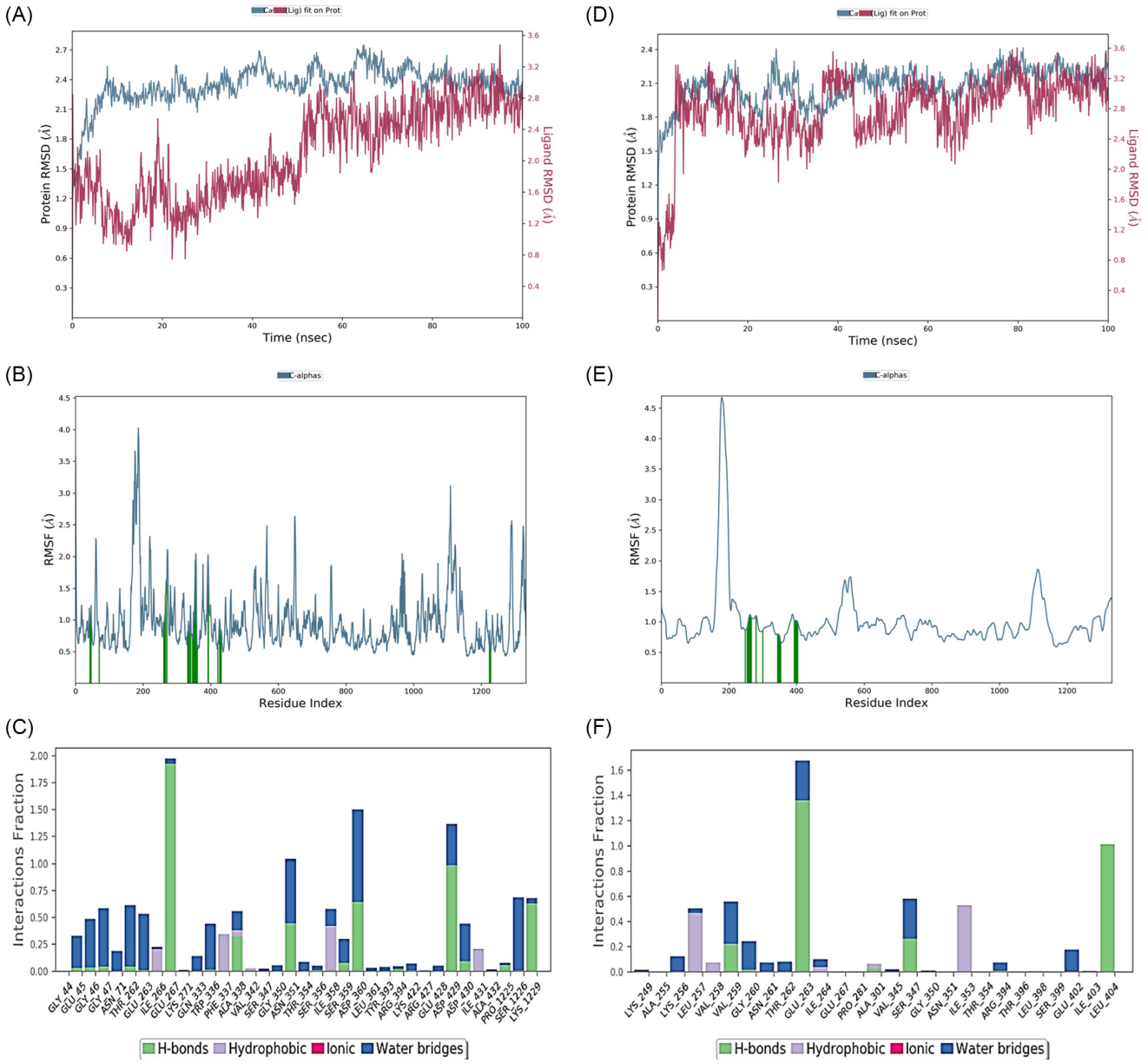

Figure 4. MD simulation results (A) RMSD of orientin and P47989 (XDH). (B) RMSF of P47989 (XDH) on binding to orientin. (C) Orientin and P47989 (XDH) contact profile. (D) RMSD of quercetin and P47989 (XDH). (E) RMSF of P47989 (XDH) on binding to quercetin. (F) Quercetin and P47989 (XDH) contact profile.

drugs out of cells. P-gp can influence drug bioavailability, and its inhibition or modulation is a consideration in drug development to enhance drug efficacy [25].

Target prediction identified several proteins potentially modulated by *C. citratus* phytochemicals. XDH is involved in purine metabolism, where it catalyzes the metabolism of hypoxanthine to uric acid and xanthine. Dysregulation of XDH is associated with conditions like hypertension, hyperuricemia, renal failure gout, diabetes, and cardiovascular problems [26]. MMP9, a member of the matrix metalloproteinase family, and dysregulation of MMP9 has been associated with various diseases, including cancer, cardiovascular diseases, inflammation, and neurodegenerative disorders [27, 28]. Targeting MMP9 at the catalytic site could be less favorable, with its activity possibly induced by long-range conformational transitions when an activator protein or ligand binds to an allosteric area [29, 30].

Some kinases were predicted to be involved in the regulation of *C. citratus* phytochemicals molecular targets, with the MAPK/ERK pathway being a common theme. This pathway is very essential for cellular processes while its dysregulation has been implicated in various diseases, notably cancer. Additionally, kinases like AKT1 may intersect with the PI3K/AKT pathway, further influencing disease processes. Similarly, certain transcription factors were predicted to be involved in the mechanism of action of *C. citratus* phytochemicals, with pathways such as Wnt, TGF-β, MAPK, and PI3K/Akt being implicated in disease states.

Molecular docking studies allow for the exploration of the binding interactions between the phytochemicals and their putative molecular targets, providing valuable information on the affinity and specificity of these interactions. This knowledge aids in the selection and optimization of lead compounds for further

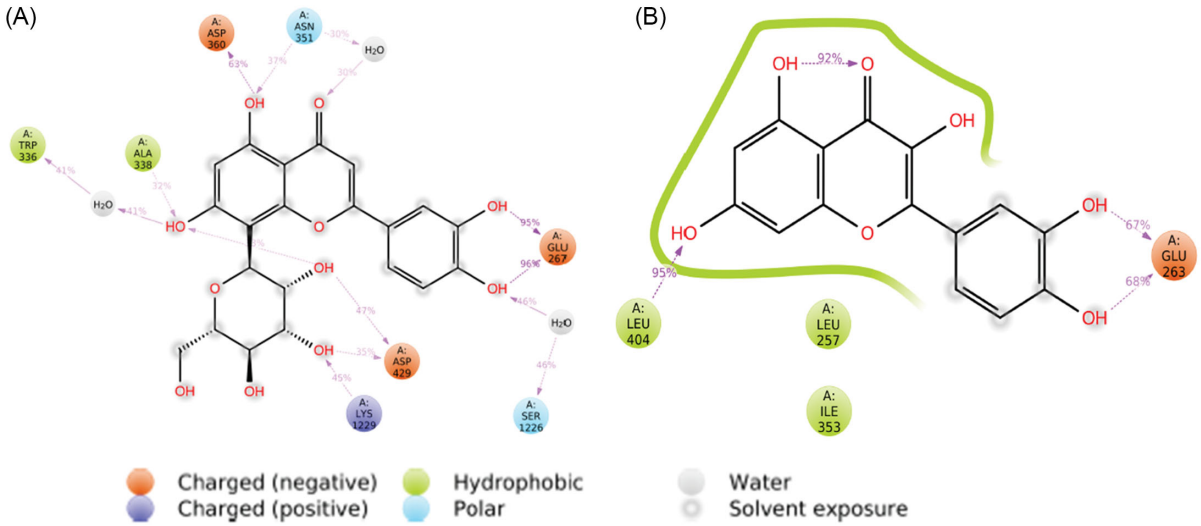

Figure 5. A representation of detailed interactions of (A) orientin and P47989 (XDH). (B) Quercetin and P47989 (XDH).

Table 4. The binding energy (ΔG^{bind}) of the interaction of XDH with orientin and quercetin respectively, at 0 and 100 ns

Complex	Simulation Time (ns)	MM-GBSA ΔG (kcal.mol^{-1})							
		Lipo	Hbond	Covalent	Solv_GB	Packing	vdW	Coulomb	ΔG^{bind} (Total)
Orientin and P47989 **(XDH)**	0	−11.535	−4.605	7.080	41.865	−1.731	−48.080	−37.332	−54.338
	100	−13.552	−4.802	2.998	34.667	−1.186	−43.353	−21.304	−46.531
Quercetin and P47989 **(XDH)**	0	−9.931	−3.180	2.498	19.221	0	−44.036	−25.761	−61.189
	100	−7.942	−1.080	0.816	23.881	0	−43.828	−11.508	−39.661

Note: Total: Total binding energy (Prime energy). **Packing**: Pi-pi packing correction. **Lipo**: Lipophilic energy. **Covalent**: Covalent binding energy. **Hbond**: Hydrogen bonding energy. **Solv GB**: Generalized Born electrostatic solvation energy. **vdW**: Van der Waals energy. **Coulomb**: Coulomb energy.

development. The binding affinities obtained for orientin in this study were higher than those reported for indigocarpan towards MMP9 using AutoDock Vina. A study by Rullo et al. [31] reported the binding interaction of quercetin to Xanthine oxidase, including amino acid residues Leu1014, Val1011, Thr1010, Phe1009, Arg880, Leu873, and Glu802. In another context, dihydroxybenzoic acid binding to MMP9 involves amino acid residues Leu188 and Met422, while Leu187 is involved in the binding of quercetin to MMP9, differing from orientin. Computational studies have identified Ser470, Met422, Asp376, Arg330, and Met328, in the binding interaction of MMP9 at the PEX9 domain [32]. Additionally, Asp185-Leu188, Met247, Tyr248, Leu397, Val398, and Pro421-Tyr423, including Ala189and Leu188 residues, are in the active site of MMP-9 protein [33–35].

Furthermore, MD simulations offer a dynamic view of the behavior of phytochemicals within biological systems, elucidating their structural changes, conformational flexibility, and dynamics over time [36]. This dynamic perspective is instrumental in understanding the stability and functional implications of ligand-protein interactions, guiding the refinement of molecular models and the design of more effective therapeutics. Monitoring RMSD helps in identifying stable conformations, understanding structural transitions, and evaluating the reliability of MD simulations. Analyzing RMSF aids in identifying functionally important regions, such as binding sites or allosteric sites, understanding protein dynamics, and guiding rational drug design efforts by targeting flexible regions. Understanding protein-ligand contacts is essential for rational drug design, as it informs the optimization of ligand binding affinity and specificity, identification of druggable sites, and prediction of ligand-induced conformational changes in the protein.

MM-GBSA calculates the binding free energy of a protein-ligand complex, which represents the overall stability of the complex in solution [15]. MM-GBSA decomposes the binding free energy into individual energy terms, such as van der Waals, electrostatic, polar solvation, and nonpolar solvation energies. Analyzing these energy contributions provides insights into the driving forces and key interactions governing protein-ligand binding. Identifying dominant energy terms informs the design of ligands with optimized interactions, such as targeting specific binding pockets or optimizing hydrogen bonding interactions. In this study, the binding energy between interaction of XDH with orientin and quercetin respectively were reduced during 100 ns MDS duration, but it indicates that they possess enough stable interaction that could have definite biological effect in real physiological condition. Positive binding free energy indicates unfavorable binding, while negative binding free energy suggests favorable binding. Understanding the binding free energy helps in prioritizing ligands with the highest affinity for further experimental validation, guiding lead optimization, and predicting ligand potency.

Moreover, other studies have combined molecular docking, MD simulation, and MM-GBSA with advanced techniques such as large-scale density functional tight binding to investigate drug-protein interaction at a quantum level [21, 37, 38].

5. Conclusion

Natural molecules, like those found in *C. citratus* extract, can indeed have enormous relevance to drug development. Studies have consistently demonstrated their benefits, including efficacy and minimal side effects. This study highlights the potential of *C. citratus* extract, particularly compounds like orientin, in drug discovery for conditions such as cancer and neurodegenerative diseases by targeting XDH and MMP9. However, further research is necessary to validate the therapeutic efficacy of *C. citratus* extract or its specific phytochemicals in targeted inhibition of XDH and MMP9 to address specific disease conditions.

Conflicts of Interest

The authors declare that they have no conflicts of interest to this work.

Data Availability Statement

The SwissADME data that support the findings of this study are openly available at www.swissadme.ch, reference number [11]. The SEA Search data that support the findings of this study are openly available at www.sea.bkslab.org, reference number [12]. The STRING data that support the findings of this study are openly available at https://string-db.org, reference number [13]. The eXpression2Kinases data that support the findings of this study are openly available at https://maayanlab.cloud/X2K/, reference number [14]. The UniProt data that support the findings of this study are openly available at www.uniprot.org.

References

[1] Borges, P. H. O., Pedreiro, S., Baptista, S. J., Geraldes, C. F. G. C., Batista, M. T., Silva, M. M. C., & Figueirinha, A. (2021). Inhibition of α-glucosidase by flavonoids of *Cymbopogon citratus* (DC) Stapf. *Journal of Ethnopharmacology*, *280*, 114470. https://doi.org/10.1016/j.jep.2021.114470

[2] Wang, H., Zhang, R., Zhang, K., Chen, X., & Zhang, Y. (2022). Antioxidant, hypoglycemic and molecular docking studies of methanolic extract, fractions and isolated compounds from aerial parts of *Cymbopogon citratus* (DC.) Stapf. *Molecules*, *27*(9), 2858. https://doi.org/10.3390/molecules27092858

[3] Subramaniam, G., Yew, X. Y., & Sivasamugham, L. A. (2020). Antibacterial activity of *Cymbopogon citratus* against clinically important bacteria. *South African Journal of Chemical Engineering*, *34*, 26–30. https://doi.org/10.1016/j.sajce.2020.05.010

[4] Evbuomwan, I. O., Alejolowo, O. O., Elebiyo, T. C., Nwonuma, C. O., Ojo, O. A., Edosomwan, E. U., . . . , & Oluba, O. M. (2024). *In silico* modeling revealed phytomolecules derived from *Cymbopogon citratus* (DC.) leaf extract as promising candidates for malaria therapy. *Journal of Biomolecular Structure and Dynamics*, *42*(1), 101–118. https://doi.org/10.1080/07391102.2023.2192799

[5] Johnson, T. O., Ojo, O. A., Ikiriko, S., Ogunkua, J., Akinyemi, G. O., Rotimi, D. E., . . . , & Adegboyega, A. E. (2021). Biochemical evaluation and molecular docking assessment of *Cymbopogon citratus* as a natural source of acetylcholine esterase (AChE)-targeting insecticides. *Biochemistry and Biophysics Reports*, *28*, 101175. https://doi.org/10.1016/j.bbrep.2021.101175

[6] Bharti, S. K., Kumar, A., Prakash, O., Krishnan, S., & Gupta, A. K. (2013). Essential oil of *Cymbopogon citratus* against diabetes: Validation by *in vivo* experiments and computational studies. *Journal of Bioanalysis & Biomedicine*, *5*(5), 194–203. https://doi.org/10.4172/1948-593X.1000098

[7] Boaduo, N. K. K., Katerere, D., Eloff, J. N., & Naidoo, V. (2014). Evaluation of six plant species used traditionally in the treatment and control of diabetes mellitus in South Africa using *in vitro* methods. *Pharmaceutical Biology*, *52*(6), 756–761. https://doi.org/10.3109/13880209.2013.869828

[8] Falode, J. A., Olofinlade, T. B., Fayeun, G. S., Adeoye, A. O., Bamisaye, F. A., Ajuwon, O. R., & Obafemi, T. O. (2023). Free and bound phenols from *Cymbopogon citratus* mitigated hepatocellular injury in streptozotocin-induced type 1 diabetic male rats via decrease in oxidative stress, inflammation, and other risk markers. *Pharmacological Research-Modern Chinese Medicine*, *7*, 100234. https://doi.org/10.1016/j.prmcm.2023.100234

[9] Madden, J. C., Enoch, S. J., Paini, A., & Cronin, M. T. D. (2020). A review of *in silico* tools as alternatives to animal testing: Principles, resources and applications. *Alternatives to Laboratory Animals*, *48*(4), 146–172. https://doi.org/10.1177/0261192920965977

[10] Fatoki, T. H., Ibraheem, O., Ogunyemi, I. O., Akinmoladun, A. C., Ugboko, H. U., Adeseko, C. J., . . . , & Enibukun, J. M. (2021). Network analysis, sequence and structure dynamics of key proteins of coronavirus and human host, and molecular docking of selected phytochemicals of nine medicinal plants. *Journal of Biomolecular Structure and Dynamics*, *39*(16), 6195–6217. https://doi.org/10.1080/07391102.2020.1794971

[11] Daina, A., Michielin, O., & Zoete, V. (2017). SwissADME: A free web tool to evaluate pharmacokinetics, drug-likeness and medicinal chemistry friendliness of small molecules. *Scientific Reports*, *7*(1), 42717. https://doi.org/10.1038/srep42717

[12] Keiser, M. J., Roth, B. L., Armbruster, B. N., Ernsberger, P., Irwin, J. J., & Shoichet, B. K. (2007). Relating protein pharmacology by ligand chemistry. *Nature Biotechnology*, *25*(2), 197–206. https://doi.org/10.1038/nbt1284

[13] Szklarczyk, D., Gable, A. L., Nastou, K. C., Lyon, D., Kirsch, R., Pyysalo, S., . . . , & von Mering, C. (2021). The STRING database in 2021: Customizable protein–protein networks, and functional characterization of user-uploaded gene/measurement sets. *Nucleic Acids Research*, *49*(D1), D605–D612. https://doi.org/10.1093/nar/gkaa1074

[14] Clarke, D. J. B., Kuleshov, M. V., Schilder, B. M., Torre, D., Duffy, M. E., Keenan, A. B., . . . , & Ma'ayan, A. (2018). eXpression2Kinases (X2K) Web: Linking expression signatures to upstream cell signaling networks. *Nucleic Acids Research*, *46*(W1), W171–W179. https://doi.org/10.1093/nar/gky458

[15] Fatoki, T. H., Faleye, B. C., Nwagwe, O. R., Awofisayo, O. A., Adeseko, C. J., Jeje, T. O., . . . , & Omuekwu, N. F. (2024). Friedelin could moderately modulate human carbonic anhydrases: An *in Silico* study. *Biointerface Research in Applied Chemistry*, *14*(2), 49.

[16] Morris, G. M., Huey, R., Lindstrom, W., Sanner, M. F., Belew, R. K., Goodsell, D. S., & Olson, A. J. (2009). AutoDock4 and AutoDockTools4: Automated docking with selective receptor

flexibility. *Journal of Computational Chemistry*, *30*(16), 2785–2791. https://doi.org/10.1002/jcc.21256

[17] Trott, O., & Olson, A. J. (2010). AutoDock Vina: Improving the speed and accuracy of docking with a new scoring function, efficient optimization, and multithreading. *Journal of Computational Chemistry*, *31*(2), 455–461. https://doi.org/10.1002/jcc.21334

[18] Eberhardt, J., Santos-Martins, D., Tillack, A. F., & Forli, S. (2021). AutoDock Vina 1.2.0: New docking methods, expanded force field, and python bindings. *Journal of Chemical Information and Modeling*, *61*(8), 3891–3898. https://doi.org/10.1021/acs.jcim.1c00203

[19] Tao, A., Huang, Y., Shinohara, Y., Caylor, M. L., Pashikanti, S., & Xu, D. (2019). ezCADD: A rapid 2D/3D visualization-enabled web modeling environment for democratizing computer-aided drug design. *Journal of Chemical Information and Modeling*, *59*(1), 18–24. https://doi.org/10.1021/acs.jcim.8b00633

[20] Bowers, K. J., Chow, E., Xu, H., Dror, R. O., Eastwood, M. P., Gregersen, B. A., . . . , & Shaw, D. E. (2006). Scalable algorithms for molecular dynamics simulations on commodity clusters. In *Proceedings of the 2006 ACM/IEEE Conference on Supercomputing*, 84-es. https://doi.org/10.1145/1188455.1188544

[21] Ali, I., Iqbal, M. N., Ibrahim, M., Haq, I. U., Alonazi, W. B., & Siddiqi, A. R. (2023). Computational exploration of novel ROCK2 inhibitors for cardiovascular disease management; insights from high-throughput virtual screening, molecular docking, DFT and MD simulation. *PLOS ONE*, *18*(11), e0294511. https://doi.org/10.1371/journal.pone.0294511

[22] Schrödinger. (2022). *What do all the prime MM-GBSA energy properties mean?* Retrieved from: https://support.schrodinger.com/s/article/1875

[23] Martin, P., Giardiello, M., McDonald, T. O., Rannard, S. P., & Owen, A. (2013). Mediation of *in vitro* cytochrome P450 activity by common pharmaceutical excipients. *Molecular Pharmaceutics*, *10*(7), 2739–2748. https://doi.org/10.1021/mp400175n

[24] Arnott, J. A., & Planey, S. L. (2012). The influence of lipophilicity in drug discovery and design. *Expert Opinion on Drug Discovery*, *7*(10), 863–875. https://doi.org/10.1517/17460441.2012.714363

[25] Fatoki, T. H., Ibraheem, O., Awofisayo, O. A., Oyedele, A. S., & Akinlolu, O. S. (2020). *In silico* investigation of first-pass effect on selected small molecule excipients and structural dynamics of P-glycoprotein. *Bioinformatics and Biology Insights*, *14*. https://doi.org/10.1177/1177932220943183

[26] Vijeesh, V., Vysakh, A., Jisha, N., & Latha, M. S. (2023). An *in silico* molecular docking and ADME analysis of naturally derived biomolecules against xanthine oxidase: A novel lead for antihyperuricemia treatment. *Biointerface Research in Applied Chemistry*, *13*(4), 327. https://doi.org/10.33263/BRIAC134.327

[27] Stankovic, S., Konjevic, G., Gopcevic, K., Jovic, V., Inic, M., & Jurisic, V. (2010). Activity of MMP-2 and MMP-9 in sera of breast cancer patients. *Pathology – Research and Practice*, *206*(4), 241–247. https://doi.org/10.1016/j.prp.2009.12.003

[28] Zheng, S., Chang, Y., Hodges, K. B., Sun, Y., Ma, X., Xue, Y., . . . , & Cheng, L. (2010). Expression of *KISS1* and MMP-9 in non-small cell lung cancer and their relations to metastasis and survival. *Anticancer Research*, *30*(3), 713–718. https://ar.iiarjournals.org/content/30/3/713.full

[29] Roeb, E., Behrmann, I., Grötzinger, J., & Breuer, B. (2000). An MMP-9 mutant without gelatinolytic activity as a novel TIMP-1-antagonist. *The FASEB Journal*, *14*(12), 1671–1673. https://doi.org/10.1096/fj.99-0947fje

[30] Adhipandito, C. F., Ludji, D. P. K. S., Aprilianto, E., Jenie, R. I., Al-Najjar, B., & Hariono, M. (2019). Matrix metalloproteinase9 as the protein target in anti-breast cancer drug discovery: An approach by targeting hemopexin domain. *Future Journal of Pharmaceutical Sciences*, *5*, 1. https://doi.org/10.1186/s43094-019-0001-1

[31] Rullo, R., Cerchia, C., Nasso, R., Romanelli, V., Vendittis, E. D., Masullo, M., & Lavecchia, A. (2023). Novel reversible inhibitors of xanthine oxidase targeting the active site of the enzyme. *Antioxidants*, *12*(4), 825. https://doi.org/10.3390/antiox12040825

[32] Remacle, A. G., Golubkov, V. S., Shiryaev, S. A., Dahl, R., Stebbins, J. L., Chernov, A. V., . . . , & Strongin, A. Y. (2012). Novel MT1-MMP small-molecule inhibitors based on insights into hemopexin domain function in tumor growth. *Cancer Research*, *72*(9), 2339–2349. https://doi.org/10.1158/0008-5472.CAN-11-4149

[33] Tochowicz, A., Maskos, K., Huber, R., Oltenfreiter, R., Dive, V., Yiotakis, A., . . . , & Goettig, P. (2007). Crystal structures of MMP-9 complexes with five inhibitors: Contribution of the flexible Arg424 side-chain to selectivity. *Journal of Molecular Biology*, *371*(4), 989–1006. https://doi.org/10.1016/j.jmb.2007.05.068

[34] Rathee, D., Lather, V., Grewal, A. S., & Dureja, H. (2018). Targeting matrix metalloproteinases with novel diazepine substituted cinnamic acid derivatives: Design, synthesis, *in vitro* and *in silico* studies. *Chemistry Central Journal*, *12*, 41. https://doi.org/10.1186/s13065-018-0411-8

[35] Malekipour, M. H., Shirani, F., Moradi, S., & Taherkhani, A. (2023). Cinnamic acid derivatives as potential matrix metalloproteinase-9 inhibitors: Molecular docking and dynamics simulations. *Genomics & Informatics*, *21*(1), e9. https://doi.org/10.5808/gi.22077

[36] Karplus, M., & McCammon, J. A. (2002). Molecular dynamics simulations of biomolecules. *Nature Structural & Molecular Biology*, *9*(9), 646–652. https://doi.org/10.1038/nsb0902-646

[37] Allec, S. I., Sun, Y., Sun, J., Chang, C. E. A., & Wong, B. M. (2019). Heterogeneous CPU+GPU-enabled simulations for DFTB molecular dynamics of large chemical and biological systems. *Journal of Chemical Theory and Computation*, *15*(5), 2807–2815. https://doi.org/10.1021/acs.jctc.8b01239

[38] Sepay, N., Chakrabarti, S., Afzal, M., Alarifi, A., & Mal, D. (2022). Identification of 4-acrylamido-N-(pyridazin-3-yl) benzamide as anti-COVID-19 compound: A DFTB, molecular docking, and molecular dynamics study. *RSC Advances*, *12*(37), 24178–24186. https://doi.org/10.1039/D2RA04333E

How to Cite: Ajayi, I. I., Fatoki, T. H., Alonge, A. S., Saliu, I. O., Odesanmi, O. E., Akinyelu, J., & Oke, O. E. (2024). ADME, Molecular Targets, Docking, and Dynamic Simulation Studies of Phytoconstituents of *Cymbopogon citratus* (DC.). *Medinformatics*, *1*(3), 152–163. https://doi.org/10.47852/bonviewMEDIN42022711